

8-20-2018

Fermi GBM Observations of GRB 150101B: A Second Nearby Event with a Short Hard Spike and a Soft Tail

E. Burns

NASA Goddard Space Flight Center

P. Veres

Center for Space Plasma and Aeronomic Research

V. Connaughton

Huntsville Program Office

J. Racusin

The University of Alabama in Huntsville

M. S. Briggs

Center for Space Plasma and Aeronomic Research

See next page for additional authors

Follow this and additional works at: https://digitalcommons.lsu.edu/physics_astronomy_pubs

Recommended Citation

Burns, E., Veres, P., Connaughton, V., Racusin, J., Briggs, M., Christensen, N., Goldstein, A., Hamburg, R., Kocevski, D., McEnery, J., Bissaldi, E., Canton, T., Cleveland, W., Gibby, M., Hui, C., Kienlin, A., Mailyan, B., Paciesas, W., Roberts, O., Siellez, K., Stanbro, M., & Wilson-Hodge, C. (2018). Fermi GBM Observations of GRB 150101B: A Second Nearby Event with a Short Hard Spike and a Soft Tail. *Astrophysical Journal Letters*, 863 (2) <https://doi.org/10.3847/2041-8213/aad813>

This Article is brought to you for free and open access by the Department of Physics & Astronomy at LSU Digital Commons. It has been accepted for inclusion in Faculty Publications by an authorized administrator of LSU Digital Commons. For more information, please contact ir@lsu.edu.

Authors

E. Burns, P. Veres, V. Connaughton, J. Racusin, M. S. Briggs, N. Christensen, A. Goldstein, R. Hamburg, D. Kocevski, J. McEnery, E. Bissaldi, T. Dal Canton, W. H. Cleveland, M. H. Gibby, C. M. Hui, A. Von Kienlin, B. Mailyan, W. S. Paciesas, O. J. Roberts, K. Siellez, M. Stanbro, and C. A. Wilson-Hodge



Fermi GBM Observations of GRB 150101B: A Second Nearby Event with a Short Hard Spike and a Soft Tail

E. Burns¹, P. Veres² , V. Connaughton³, J. Racusin¹ , M. S. Briggs^{2,4}, N. Christensen^{5,6}, A. Goldstein³ , R. Hamburg^{2,4}, D. Kocevski⁷, J. McEnery¹, E. Bissaldi^{8,9} , T. Dal Canton¹, W. H. Cleveland³, M. H. Gibby¹⁰, C. M. Hui⁷, A. von Kienlin¹¹, B. Mailyan², W. S. Paciasas³ , O. J. Roberts³, K. Siellez¹², M. Stanbro⁴, and C. A. Wilson-Hodge⁷ 

¹NASA Goddard Space Flight Center, Greenbelt, MD 20771, USA; eric.burns@nasa.gov

²Center for Space Plasma and Aeronomic Research, University of Alabama in Huntsville, Huntsville, AL 35899, USA

³Science and Technology Institute, Universities Space Research Association, Huntsville, AL 35805, USA

⁴Space Science Department, University of Alabama in Huntsville, Huntsville, AL 35899, USA

⁵Physics and Astronomy, Carleton College, MN 55057, USA

⁶Artemis, Université Côte d'Azur, Observatoire Côte d'Azur, CNRS, CS 34229, F-06304 Nice Cedex 4, France

⁷Astrophysics Branch, ST12, NASA/Marshall Space Flight Center, Huntsville, AL 35812, USA

⁸Istituto Nazionale di Fisica Nucleare, Sezione di Bari, I-70126 Bari, Italy

⁹Dipartimento Interateneo di Fisica, Politecnico di Bari, Via E. Orabona 4, I-70125, Bari, Italy

¹⁰Jacobs Technology, Inc., Huntsville, AL 35805, USA

¹¹Max-Planck-Institut für extraterrestrische Physik, Giessenbachstrasse 1, D-85748 Garching, Germany

¹²Center for Relativistic Astrophysics and School of Physics, Georgia Institute of Technology, Atlanta, GA 30332, USA

Received 2018 July 13; revised 2018 August 3; accepted 2018 August 4; published 2018 August 17

Abstract

In light of the joint multimessenger detection of a binary neutron star merger as the gamma-ray burst GRB 170817A and in gravitational waves as GW170817, we reanalyze the *Fermi* Gamma-ray Burst Monitor data of one of the closest short gamma-ray bursts (SGRBs): GRB 150101B. We find that this burst is composed of a short hard spike followed by a comparatively long soft tail. This apparent two-component nature is phenomenologically similar to that of GRB 170817A. While GRB 170817A was distinct from the previously known population of SGRBs in terms of its prompt intrinsic energetics, GRB 150101B is not. Despite these differences, GRB 150101B can be modeled as a more on-axis version of GRB 170817A. Identifying a similar signature in two of the closest SGRBs suggests that the soft tail is common, but generally undetectable in more distant events. If so, it will be possible to identify nearby SGRBs from the prompt gamma-ray emission alone, aiding the search for kilonovae.

Key words: gamma-ray burst: general – gamma-ray burst: individual (GRB 150101B)

1. Introduction

Burns et al. (2016) asserted that extremely close short gamma-ray bursts (SGRBs) are not necessarily bright. The assertion is based on the lack of correlation between redshift and the prompt SGRB brightness at Earth and the modest fluence (compared to other SGRBs) of the nearby short GRB 150101B. This was potentially very important given the new era of gravitational wave (GW) astronomy and the unique science possible only with joint GW–GRB detections. This expectation was spectacularly confirmed by the joint multimessenger detection of the merging of two neutron stars in GWs as GW170817 (Abbott et al. 2017c) by Advanced Laser Interferometer Gravitational-Wave Observatory (LIGO; Aasi et al. 2015) and Advanced Virgo (Acernese et al. 2015) and in gamma-rays as the low-luminosity GRB 170817A (Goldstein et al. 2017; Savchenko et al. 2017) by the *Fermi* Gamma-ray Burst Monitor (GBM; Meegan et al. 2009) and by the SPectrometer on-board *INTEGRAL* Anti-Coincidence Shield (SPI-ACS; von Kienlin et al. 2003). The results from the joint detection confirmed binary neutron star mergers as progenitors of SGRBs and measured the speed of gravity to within one part in 10^{-15} of the speed of light (Abbott et al. 2017a). To maximize the science from multimessenger observations of

neutron star mergers, we need to identify nearby events and fully understand them. GRB 170817A falls within the normal SGRB distributions of fluence, peak flux, peak energy, and duration for SGRBs (Goldstein et al. 2017). However, it appears to be composed of a short hard spike (similar to the usual phenomenology of more distant SGRBs) followed by a longer soft tail that may be thermal in origin, falls on the softer and longer ends of the hardness and duration distributions of SGRBs (as observed with GBM; Goldstein et al. 2017), and is several orders of magnitude less luminous than other SGRBs with known redshift (Abbott et al. 2017a).

We now return to GRB 150101B. New analysis on fine timescales of this burst, presented here, uncovers a short hard spike followed by a longer soft tail that may be thermal in origin. As GRBs 170817A and 150101B are among the closest SGRBs (of those with unambiguously measured redshifts; see Abbott et al. 2017a) identifying a similar two-component signature in both bursts is intriguing. It seems unlikely to be commonly detected in the SGRB population given the lack of identification prior to GRB 170817A, despite thorough analyses of the gamma-ray data from SGRBs (Preece et al. 2000; Kaneko et al. 2006; Guiriec et al. 2010; Svinkin et al. 2016; Yu et al. 2016; Burns 2017). It is not clearly identifiable in two other close SGRBs, which is discussed in Section 5. We report here a detailed analysis of GRB 150101B. We show that it is a typical SGRB in gamma-rays, and compare it with GRB 170817A. Despite their common morphology of a harder spike followed by a softer tail, the



two bursts differ in important ways: GRB 150101B is neither subluminal nor subenergetic compared to other SGRBs, is not spectrally soft, and its total prompt duration in gamma-rays is significantly shorter than GRB 170817A. Various theoretical models have been applied to explain the unusual behavior of the prompt and afterglow emission from GRB 170817A. We briefly comment on possible applicability of some of these models to GRB 150101B and discuss possible implications for GRB 170817A.

Prior to GW170817, Fong et al. (2016) presented an analysis of GRB 150101B, concluding that the afterglow exhibited typical broadband behavior for SGRBs. A more recent analysis of these data combined with a measure of the total gamma-ray energetics asserts that GRB 150101B has a luminous blue kilonova and an off-axis jet (Troja et al. 2018b). That analysis reports a measure of the total gamma-ray energetics that differs significantly from our previously published results (Abbott et al. 2017a). Their lower value arises from the selection of a narrower energy range and the differences between the *Swift* Burst Alert Telescope (BAT) and *Fermi* GBM observations of GRB 150101B, previously investigated in Burns et al. (2016). A new understanding of the differing BAT and GBM observations of GRB 150101B is discussed in the Appendix. While investigating the differences between the GBM published values and those in Troja et al. (2018b) we discovered the characteristics of the burst presented here.

2. Observed Properties of GRB 150101B

GRB 150101B triggered GBM on-board at 2015 January 01 15:24:34.468 UTC, was reported to the community within 7 s, and cataloged with trigger ID GRB150101641 and trigger number 441818617.¹³ A ground analysis of BAT slew data identified a significant source and constrained the position to (R.A., decl.) = (188.044, -10.956) with an uncertainty of 2.5 arcmin (Cummings 2015), enabling broadband follow-up observations.

The total duration, the two-component nature, the durations of each component, and the significance of the soft tail in GRB 150101B are supported by several analysis methods. Figure 1 shows that the count rates recorded in the relevant GBM detectors as a function of time and energy are suggestive of two distinct spectral components. The counts are taken from all GBM detectors with good viewing geometry to the position of GRB 150101B at event time. These are the sodium iodide (NaI) detectors 3, 4, 6, 7, and 8 and both bismuth germanate (BGO) detectors. The reference time and combination of detectors is used throughout the analysis. The short hard spike is 16 ms long (covering the 16 ms before T₀) followed by a longer soft tail that lasts about 64 ms (covering the 64 ms after T₀), for an overall duration of about 80 ms.

The standard GBM duration parameters, which describe the time to accumulate the central 90% and 50% of the total fluence, are $T_{90} = 0.08 \pm 0.93$ s and $T_{50} = 0.016 \pm 0.023$, respectively. These duration measures include contributions from both components. All GBM catalog values are taken from the online catalog¹³. Both measures start 16 ms before the trigger time. The large uncertainties are driven by the short timescales of the event and the difficulty in applying this method to SGRBs with modest fluence, but the start times and

central values match those inferred from other methods. Few GBM SGRBs appear to have durations less than ~ 100 ms long.

The timescales of each separate component are additionally supported by results from the GBM Targeted Search (discussed in the next section) and the Bayesian Block technique (Scargle et al. 2013). Applying the latter technique to the data from the relevant GBM NaI detectors reveals the two emission episodes without any prior assumptions on timescales. In the 50–300 keV range, where GBM is most sensitive, the analysis isolates the short hard spike over the same pre-trigger 16 ms timescale as other methods. In the 10–50 keV energy range the analysis identifies the soft tail over a 73 ms interval starting at trigger time, with a significance of more than 10 sigma. This suggests that the soft tail is marginally longer than 64 ms and is consistent with the slight excess in the succeeding 16 ms bins in the low-energy counts lightcurves (Figure 1). To ensure both components arise from GRB 150101B, we localize them independently using the GBM Targeted Search method (Goldstein et al. 2017) and find that both are consistent with the known source position from Cummings (2015).

For GRBs with measured redshift and broadband spectral observations we can constrain the total intrinsic energetics. By measuring the brightness at Earth and assuming constant flux over a sphere with a radius of the distance to the source, we can measure isotropic-equivalent energetics that are measured over the bolometric 1 keV–10 MeV rest-frame energy range (Bloom et al. 2001). Some SGRBs have measured jet opening angles (Rhoads 1999; Fong et al. 2015). For collimated outflows, isotropic-equivalent energetics are overestimates of the true intrinsic energetics. The two measures are the peak luminosity L_{iso} , calculated from the peak flux, and the total energy E_{iso} , calculated from the fluence. For GRB 150101B, the GBM catalog fluence is $(2.4 \pm 0.2) \times 10^{-7}$ erg cm⁻². This fluence is taken from the analysis that derives T_{90} , as it more fully captures the fluence of the burst by accounting for spectral evolution and contribution from low-count bins. The standard time-integrated and 64 ms peak flux and fit parameters from spectral analysis are given in Table 1. All measures of flux and fluence are given over the 10–1000 keV energy range. The peak flux and fluence are converted to peak L_{iso} and E_{iso} , assuming the redshift of the associated host galaxy $z = 0.134$ (Levan 2015; Fong et al. 2016). The standard E_{iso} value for GRB 150101B is 2.3×10^{49} erg (Abbott et al. 2017a). Figure 2 shows the E_{iso} and L_{iso} distribution for GRBs, which show two SGRBs with comparable total energetics. Also shown is GRB 170817A, which is a significant outlier in both distributions (Abbott et al. 2017a).

GRB 150101B has significantly more counts in GBM than GRB 170817A, which enables more detailed spectral analysis. To explore the best spectral fits to the two components in GRB 150101B and to search for evidence of spectral evolution, the burst is divided into time slices and data from each slice analyzed separately. Details of GBM spectral analysis and a description of the functions typically used in GRB spectral fits can be found in the GBM spectral catalogs (Gruber et al. 2014). The preferred models, best-fit parameters, and fluxes from both the catalog results and the time-resolved fits are shown in Table 1 and Figure 3. The hard spike is best fit by a power law in energy with a flux that drops exponentially above a peak energy, referred to as a comptonized function. The peak energy lies close to the center of the distribution of peak energies for SGRBs detected by GBM. The soft tail is best fit by a

¹³ <https://gcn.gsfc.nasa.gov/other/441818617.fermi>

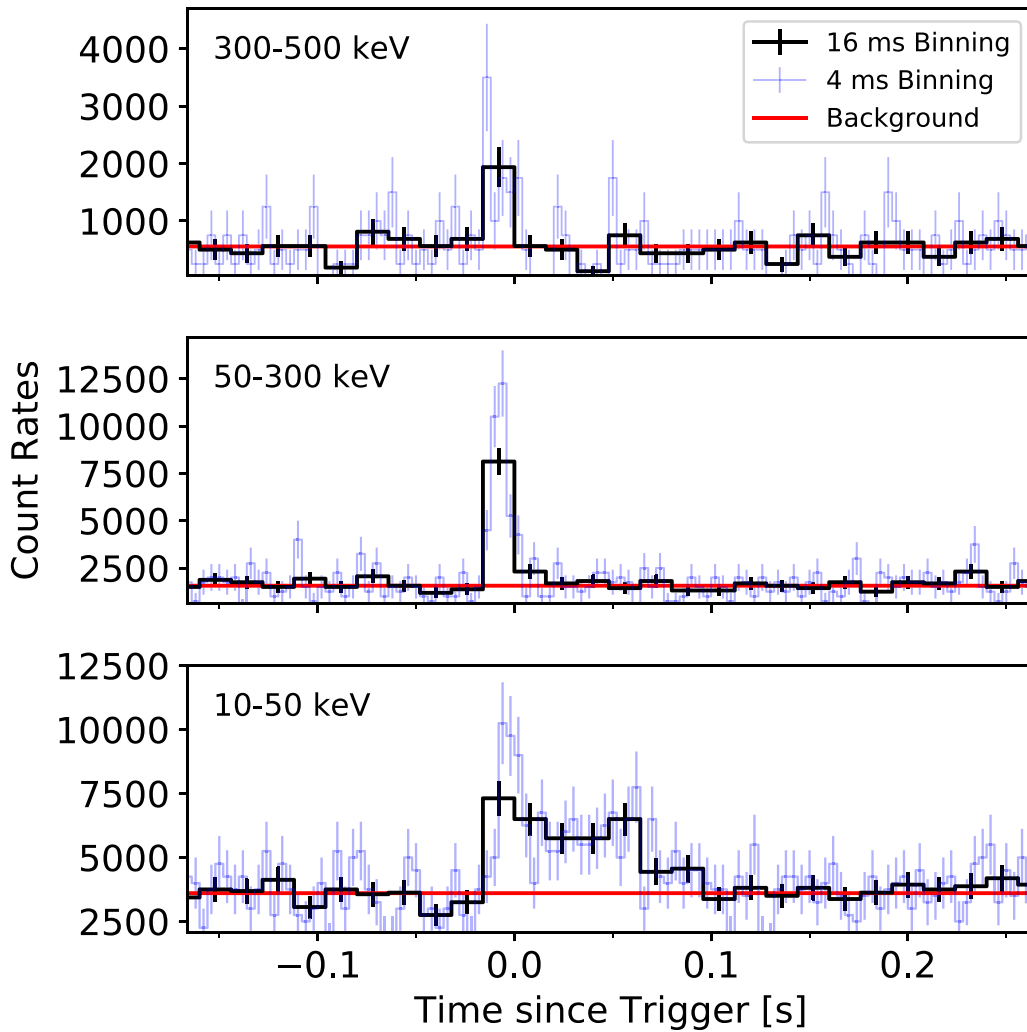


Figure 1. Count rates in different energy ranges showing the short hard spike and the longer soft tail in GRB 150101B. All ranges include counts in the NaI detectors; the counts in the BGO detectors are included only in the highest energy range. The short hard spike is visible above 50 keV. The soft tail is obvious in the 10–50 keV channel. GRB 150101B triggered GBM on the 16 ms timescale corresponding to the main peak, which places T_0 at the end of this interval. The background count rates around trigger time are flat and well behaved; the background levels shown here are the time-averaged values around the trigger.

blackbody spectrum; however, this does not mean the true spectrum is thermal. Using these best-fit functions, the fluence of the main peak is $(1.2 \pm 0.1) \times 10^{-7} \text{ erg cm}^{-2}$ and $(2.0 \pm 0.2) \times 10^{-8} \text{ erg cm}^{-2}$ for the soft tail.

From summing the time-resolved fits, the total energetics values for the main peak (MP) and soft tail (ST) are $E_{\text{iso}}^{\text{MP}} = (9.0 \pm 1.1) \times 10^{48} \text{ erg}$ and $E_{\text{iso}}^{\text{ST}} = (1.1 \pm 0.1) \times 10^{48} \text{ erg}$. The sum of the E_{iso} of the two components is about half the E_{iso} upper limit inferred from the standard analysis, confirming the standard analysis as a reliable measure. The L_{iso} values of each component, as well as sub-intervals, are given in Table 1. The very short duration of the main peak and the two-component composition complicate the standard calculation of L_{iso} for GRB 150101B. Nevertheless, $L_{\text{iso}}^{\text{MP}} \approx 4 \times 10^{50} \text{ erg s}^{-1}$, within the normal distribution of SGRBs, as evident from Figure 2.

As shown in Table 1 and Figure 3, we further resolve each component: the main peak into two 8 ms intervals and the soft tail into four 16 ms intervals. We caution against strong inferences from fits to such short timescales; we use them here to investigate possible spectral evolution. The time-resolved fits of the main peak suggest hard to soft evolution within the

pulse, seen in most GRBs (Yu et al. 2016). The time-resolved fits of the soft tail show a declining temperature, while the flux is approximately constant.

The minimum variability timescale for GRB 150101B, measured in the same manner as Golkhou et al. (2015), is $7.5 \pm 0.8 \text{ ms}$. This millisecond variability constrains the ratio of the radius (R) of the emitting region to the bulk Lorentz factor (Γ) to a value $R/\Gamma^2 < 2ct_v/(1+z) \approx 4000 \text{ km}$. With $\Gamma \approx 1200$ (the highest lower limit inferred for a SGRB, from Ackermann et al. 2010), we constrain $R < 5.7 \times 10^9 (\Gamma/1200)^2 \text{ km}$.

3. Comparison to GRB 170817A

Figure 4 shows the key features in GRBs 150101B and 170817A: a main peak characterized as a short hard spike followed by a transition to longer softer emission with a possible secondary peak, which is reasonably consistent with a thermal spectrum. This figure is generated with the GBM Targeted Search (Blackburn et al. 2015; Goldstein et al. 2016; Kocevski et al. 2018) and shows as a function of time the characteristics of the most significant signals above background revealed by the search on each of the input timescales. The

Table 1
Preferred Models and Best-fit Parameters from the Spectral Analysis of GRB 150101B

Time Range (ms)	Model	E_{peak} or kT (keV)	Index	Photon Flux $\text{ph s}^{-1} \text{cm}^{-2}$	Energy Flux $10^{-7} \text{erg s}^{-1} \text{cm}^{-2}$	$L_{\text{iso}} 10^{49} \text{erg}^{-1} \text{s}^{-1}$
Catalog						
−64:64	Power law	...	-1.8 ± 0.1	7.9 ± 0.9	8.3 ± 1.4	...
0:64	Power law	...	-2.4 ± 0.3	10.4 ± 1.4	4.8 ± 1.1	<7.5
Integrated						
−16:0	Comptonized	550 ± 190	-0.8 ± 0.2	28.3 ± 2.6	72 ± 8	44 ± 5
0:64	Blackbody	6.0 ± 0.6	...	9.3 ± 1.1	3.1 ± 0.4	1.8 ± 0.2
Resolved						
−16:−8	Comptonized	1280 ± 590	-0.4 ± 0.3	19.8 ± 2.8	96 ± 14	101 ± 15
−8:0	Comptonized	190 ± 50	-0.7 ± 0.3	36.4 ± 4.3	49 ± 8	26 ± 4
0:16	Blackbody	9.0 ± 1.3	...	10.1 ± 2.0	4.5 ± 1.0	2.4 ± 0.5
16:32	Blackbody	7.1 ± 1.6	...	7.3 ± 2.0	2.7 ± 0.8	1.5 ± 0.5
32:48	Blackbody	6.2 ± 1.5	...	8.4 ± 2.1	2.9 ± 0.7	1.7 ± 0.4
48:64	Blackbody	3.7 ± 0.7	...	12.8 ± 2.6	3.3 ± 0.7	2.5 ± 0.5

Note. For the catalog rows the −64 to +64 ms interval corresponds to the fluence measure from the GBM spectral catalog, and the 0 to +64 ms interval to the peak flux interval. We compared the standard GRB functions, a blackbody, and multi-component fits of a blackbody and a standard GRB function. Single-component fits are preferred in all intervals. The best-fit models were either a power law, a blackbody, or a comptonized spectrum; see Gruber et al. (2014) for details. E_{peak} parameterizes the peak energy for the comptonized spectrum. The L_{iso} measures for intervals less than 64 ms cannot be directly compared to other bursts.

color coding reflects the spectral template favored by the transient, and the intensity maps the log likelihood ratio that a source is preferred over just background in that time interval.

For GRB 150101B the search identifies the soft tail most significantly on the 64 ms timescale starting at T0. The signal in this source window has a log likelihood ratio of about 60 for the very soft thermal spectral template, which is more significant than several GBM-triggered SGRBs (Kocevski et al. 2018). The hard spike is found with maximal significance in the 16 ms source window ending at trigger time, with a log likelihood ratio that is greater than 400. These source windows of maximum significance match the durations and phases previously inferred by visual inspection of the counts light-curves and the Bayesian Blocks analysis, providing additional evidence for the two components. The transition from the main peak to the thermal-like tail is stark for GRB 150101B, occurring immediately once the 64 ms source window no longer overlaps with the main peak. The fast transition and the soft tail persisting for several times the duration of the main peak is unlike typical hard to soft evolution observed in GRB pulses (Yu et al. 2016).

However, there are important differences between GRBs 150101B and 170817A. GRB 170817A has intrinsic isotropic energetics several orders of magnitude below any other SGRB with known redshift; GRB 150101B does not. The ratios of the peak luminosities of the main peak to the soft tail in GRB 150101B are far greater than the factor of a few difference for GRB 170817A (Abbott et al. 2017a). The main peak of GRB 150101B appears to have a higher peak energy than that of GRB 170817A, but they are roughly consistent within errors (GRB 170817A also shows spectrally harder intervals in time-resolved analysis; see Veres et al. 2018). The greatest difference between the two bursts inferred from GBM data alone is the absolute timescale: GRB 150101B has an observed duration more than an order of magnitude shorter than GRB 170817A.

4. The Origin of the Soft Tail

Historically, GRBs have been modeled as uniform top-hat jets because they sufficiently explained observations. When jets plow through dense environments they deposit a fraction of their energy in a hot cocoon (Ramirez-Ruiz et al. 2002; Pe’er et al. 2006), which may occur in binary neutron star mergers as the ultrarelativistic jet that powers the SGRB pushes through material ejected just before merger (Lazzati et al. 2017). GRB 170817A has odd behavior in both prompt and afterglow emission, the origin of which is a matter of some debate (Abbott et al. 2017a; Alexander et al. 2017, 2018; Bromberg et al. 2017; Haggard et al. 2017; Kasliwal et al. 2017; Margutti et al. 2017; Mooley et al. 2018a, 2018b; Troja et al. 2017, 2018a; Gottlieb et al. 2018; Lazzati et al. 2018; Lyman et al. 2018; Nakar & Piran 2018; Nynka et al. 2018; Ruan et al. 2018; Veres et al. 2018). Possible interpretations include a structured ultrarelativistic jet (e.g., Alexander et al. 2018), a jet and cocoon together (e.g., Abbott et al. 2017a), or a cocoon model (e.g., Kasliwal et al. 2017) where the shock breakout produces the harder peak. Possible mechanisms for the soft tail include the photosphere of the jet or arising from the photosphere of the cocoon.

Some argue that both the main peak and soft tail of GRB 170817A can be explained by cocoon shock breakout models (Gottlieb et al. 2017; Kasliwal et al. 2017). For GRB 150101B $L_{\text{iso}}^{\text{MP}} \sim 4 \times 10^{50} \text{erg s}^{-1}$, the L_{iso} ratio is ~ 25 , and the duration is an order of magnitude shorter than 0.5 s, all of which appear inconsistent with the simulations in Gottlieb et al. (2017). The properties of the shock breakout emission are determined by the radius where the breakout occurs and the shock velocity. From this, it follows that there should be a relation between observables such as duration, total energy, and typical energy (Nakar & Sari 2012): $T_{90} \approx 1 \text{ s} (E/10^{49} \text{erg})^{1/2} (E_{\text{peak}}/550 \text{keV})^{-2.68}$. For GRB 150101B, the duration $<0.1 \text{ s}$, which is incompatible with the cocoon shock breakout model. The soft tail with typical energy of $3.9 \times 6.0 kT \sim 23 \text{ keV}$ and similar duration is even more inconsistent with the above relation. This conclusively excludes

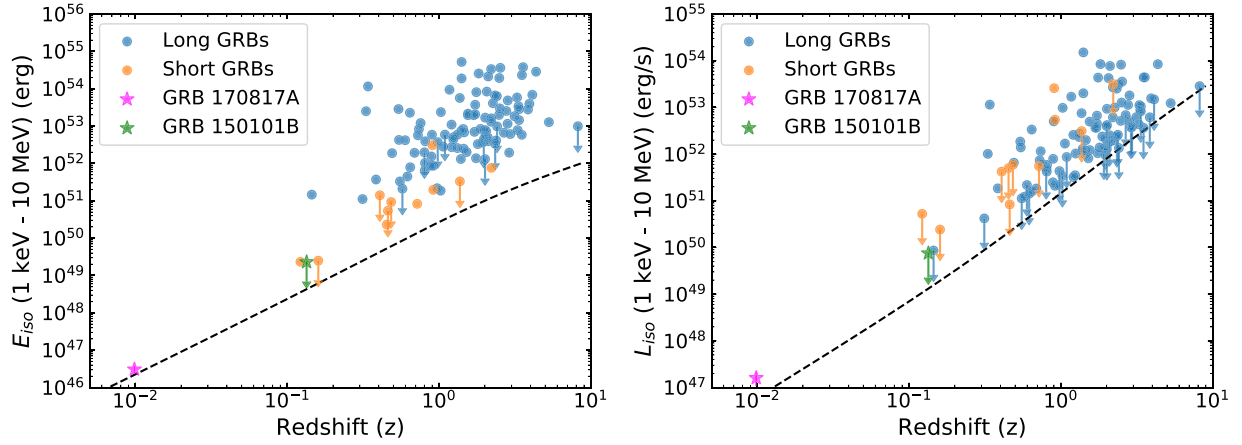


Figure 2. Isotropic-equivalent energetics for GBM GRBs with redshifts. This is a modified version of a figure in Abbott et al. (2017a). The total energetics (E_{iso}) is shown on the left and the 64 ms peak luminosity (L_{iso}) on the right. Both are given over the bolometric energy range from 1 keV to 10 MeV. GRBs best fit by a spectral model that constrains spectral curvature are shown as points. Power-law fits do not constrain spectral curvature and therefore overestimate the true value. GRBs best fit by a power law are shown as upper limits. The dashed black line is an approximate threshold for triggering GBM on-board.

cocoon shock breakout as the origin of the main peak of GRB 150101B. However, the soft tail may arise from the photosphere of the wide-angle cocoon during the brightest phase.

Afterglow observations of GRB 170817A 200–300 days post-merger show a turnover in the temporal decay from X-ray to radio that appears to favor the structured jet scenario over the cocoon scenario (Alexander et al. 2018). The very long baseline interferometry measurements of the movement of the core of the radio emission do as well (Mooley et al. 2018a). If the components in GRBs 150101B and 170817A are indeed similar, our analysis of the main peak of GRB 150101B adds additional evidence against the observed non-thermal emission originating entirely from a cocoon.

In GRB 150101B, the onset of the soft tail emission begins at least by the end of the main peak, but may occur earlier and be hidden by the main peak. This suggests that the significantly more energetic main peak and the soft emission have a common origin. While the absolute timescales of the two bursts differ greatly, the relative timescales are similar: the duration of the soft tail is about four times as long as the duration of the main peak and the possible secondary, very soft peak arises at the end of this interval. The long and softer observed characteristics of GRB 170817A could be a result of timescale broadening, $Dt \propto 1 + (\Gamma \theta_{\text{off-axis}})^2$ (Abbott et al. 2017a). This is consistent with the inclination angle inferred from multi-messenger observations (Abbott et al. 2018a; Finstad et al. 2018) and follow-up observations of the non-thermal emission (Margutti et al. 2017; Mooley et al. 2018a). The short minimum variability timescale for GRB 150101B suggests a high Γ (Sonbas et al. 2015) and the higher luminosity would be expected for a more on-axis or fully on-axis alignment. If both components emit from the structured jet then they would be significantly broadened for GRB 170817A but not for GRB 150101B, resulting in large differences in absolute timescales but not in the relative timescales of the two components. Therefore, this interpretation is self-consistent for both bursts. One physical model for both components arising from the jet is an external shock origin for the main peak and a photospheric origin for the soft tail (Abbott et al. 2017a). Subdominant spectral components that are consistent with a thermal origin are often observed during the main peak of GRBs and generally attributed to photospheric emission (Ryde 2005). The soft tail

would follow the main peak if the photospheric radius is larger than the deceleration radius (Abbott et al. 2017a).

We here demonstrate that this model can explain GRB 150101B. The innermost stable circular orbit for a $2.8 M_{\odot}$ black hole (roughly the total mass of GW170817; Abbott et al. 2017c) is $R_0 = 2.5 \times 10^6$ cm. We can rewrite this as $R_0 = 10^{6.4} R_{0,6.4}$ cm, a notation that we use in the following derivation. A jet launched at $R_{0,6.4}$ with a total luminosity $L_0 = 10^{51} L_{0,51} \text{ erg s}^{-1}$ will have an initial temperature of $kT_0 = k(L_0/4\pi R_0^2 \text{ ca})^{1/4} = 1.3 L_{0,51}^{1/4} R_{0,6.4}^{-1/2} \text{ MeV}$, with the radiation constant $a = 7.57 \times 10^{-18} \text{ kg s}^{-1} \text{ cm}^{-2} \text{ K}^{-4}$. The jet accelerates as $\Gamma \propto R/R_0$ until it reaches the saturation radius $R_{\text{sat}} = \eta R_0 = 7.2 \times 10^8 \eta_{2.5} R_{0,6.4}$ cm, with η being the dimensionless entropy of the fireball (which is generally above ~ 100 to prevent the compactness problem; Goodman 1986).

The jet becomes optically thin at the photospheric radius $R_{\text{phot}} = L\sigma_T/4\pi m_p c^3 \eta^3 = 4.3 \times 10^{10} L_{0,51} \eta_{2.5}^{-3}$ cm (when neglecting pairs; Mészáros & Rees 2000), with σ_T the Thomson cross section and m_p the mass of the proton. Here the photosphere occurs during the coasting phase ($R_{\text{sat}} < R_{\text{phot}}$), giving an observed temperature $kT_{\text{obs}} = kT_0(R_{\text{phot}}/R_{\text{sat}})^{-2/3} = 3.5 L_{0,51}^{-5/12} \eta_{2.5}^{8/3} R_{0,6.4}^{1/6} \text{ keV}$ and $L_{\text{phot}} = L_0(R_{\text{phot}}/R_{\text{sat}})^{-2/3} = 2.7 \times 10^{48} L_{0,51}^{1/3} \eta_{2.5}^{8/3} R_{0,6.4}^{2/3} \text{ erg s}^{-1}$. For fiducial values $L_0 \approx 6.1 \times 10^{51} R_{0,6.4}^{-2/3} \text{ erg s}^{-1}$ (L_0 exceeds L_{iso} because it also converts into the kinetic energy of the jet) and $\eta \approx 160 R_{0,6.4}^{-1/6}$ in the above equations, we recover the observed $kT_{\text{obs}} = 6 \text{ keV}$ and $L_{\text{phot}} = 1.8 \times 10^{49} \text{ erg s}^{-1}$.

Lastly, we derive the condition for the photospheric radius to occur above the deceleration radius. The density in the close vicinity of a neutron star merger can be approximated as a wind medium (e.g., Bauswein et al. 2013). The number density can be written as $n(R) = AR^{-2}$ where $A = \dot{M}/4\pi m_p v$, with v the outflow velocity of the wind and \dot{M} is the mass-loss rate. The deceleration radius, where the jet slows down significantly is: $R_{\text{dec}} = E_k/4\pi m_p c^2 A \eta^2$ where E_k is the kinetic energy of the outflow (Panaitescu & Kumar 2000). For $R_{\text{dec}} \lesssim R_{\text{phot}}$, $A \gtrsim 4.5 \times 10^{35} \eta_2 E_{k,50} L_{0,51}^{-1}$. This corresponds to a mass density $\rho \gtrsim 10^{-2} (R/100 \text{ km})^{-2} \text{ g cm}^{-3}$, which is consistent with simulations (Bauswein et al. 2013). Therefore, the condition for the soft tail arising from photospheric emission and being emitted at a larger radius than the external shocks

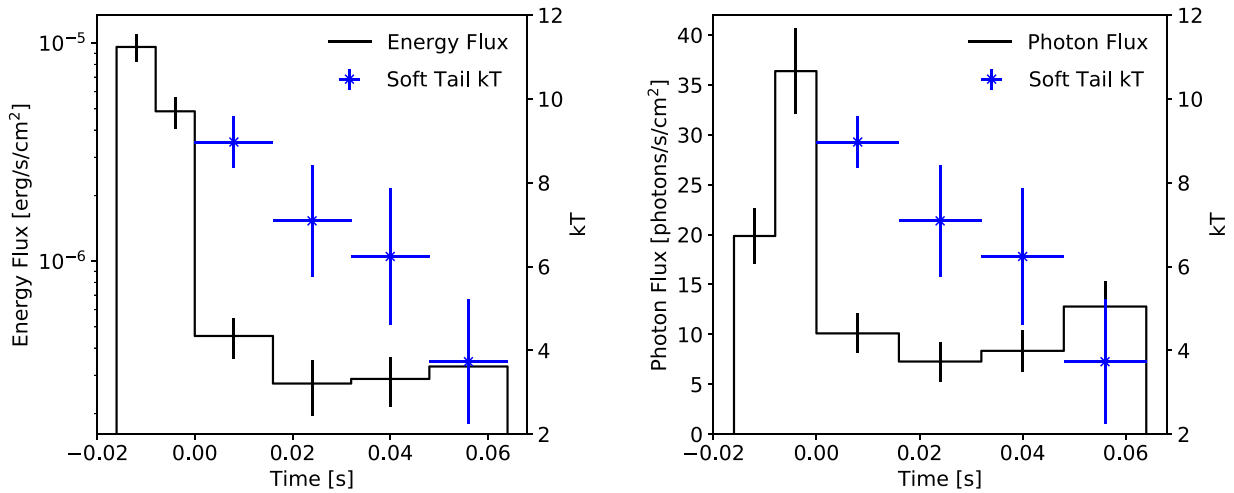


Figure 3. Deconvolved lightcurves of GRB 150101B in energy flux (left) and photon flux (right) shown in black. The main peak has significantly higher flux than the soft tail. The fits to the soft tail show a declining temperature, while the flux appears constant.

that produce the main peak matches expectations for BNS mergers. We conclude this model can explain GRB 150101B, as well as GRB 170817A (as shown in Abbott et al. 2017a).

5. The Nature and Detectability of the Soft Tail

While the significance of the soft tail in GRB 150101B is unambiguous (>10 sigma, according to the Bayesian Blocks analysis), its origin is uncertain. There is evidence in favor of the soft tail originating from thermal emission: there is a statistical preference for a blackbody spectrum (over standard GRB functions) in both the time-integrated and time-resolved fits of the soft tail, the parameters of a comptonized spectrum being similar to those that would arise from a thermal component (high index, matching peak energies), and evidence of cooling. Together this suggests that the tail may have a thermal origin, but it is not conclusive. The forward-folding technique can only measure the consistency of the data with an assumed function and other emission mechanisms or multi-temperature emission zones may result in blackbody-like emission and evolution to softer values. Therefore, just as for GRB 170817A, we cannot be certain that the soft tail is thermal in nature (Goldstein et al. 2017).

Figure 3 and Table 1 show the evidence for cooling in the soft tail. GBM can constrain blackbody temperatures down to $kT \sim 3$ keV (Jenke et al. 2016), the last of the four 16 ms bins of the soft tail has a temperature of about 4 keV, and the next two 16 ms bins are ~ 2 sigma above background in the lowest energy range. All of this is consistent with a blackbody at ~ 10 keV just after T_0 , which cools out of detectability in less than 100 ms. If the soft tail is not thermal this statement likely still holds, as a blackbody spectrum reasonably captures its behavior. If true, we detect the soft emission for GRB 150101B only because the main emission is extremely short. More generally, soft emission would be unidentifiable in SGRBs if it cools out of detectability before the dominant non-thermal emission ends. However, this would also require the unbroadened tail of GRB 170817A to be detectable longer than the main emission episode.

Ground-based GW interferometers quantify their sensitivity by the detection range of canonical BNS ($1.4 M_{\odot}$) mergers (see, e.g., Abbott et al. 2018b). GW interferometers have position-dependent sensitivities; the range is the radius of the spherical

equivalent volume to which a given interferometer is sensitive. The updated BNS merger detection range for Advanced LIGO is 173 Mpc (Barsotti et al. 2018). The most distant events that can be detected are face-on mergers at the position of the maximal antenna pattern sensitivity, which is 2.26 times the detection range (when cosmological effects can be neglected; Finn & Chernoff 1993). Joint GW-GRB detections can extend this range by $\sim 20\%$ – 25% (Williamson et al. 2014; Blackburn et al. 2015; Abbott et al. 2017b). Altogether, the joint GW-GRB detection horizon of Advanced LIGO at design sensitivity is ~ 500 Mpc ($z \approx 0.1$; Burns 2017). GRB 150101B occurred at a redshift of 0.134 (Levan 2015), corresponding to a luminosity distance of ~ 650 Mpc (using standard cosmology from Planck Collaboration et al. 2016), somewhat beyond where Advanced LIGO could detect a BNS merger. Using a nominal signal-to-noise ratio threshold of ~ 5.4 (Goldstein et al. 2017), the GBM Targeted Search could recover the main peak to ~ 1500 Mpc, and the soft tail to ~ 900 Mpc. With the most sensitive search for short gamma-ray transients, the main peak of GRB 150101B has a detectable volume five times as large as the soft tail.

Two other close SGRBs are GRB 080905A and GRB 160821B. GRB 080905A has an associated host galaxy at $z = 0.1218$ (Rowlinson et al. 2010). GRB 160821B has an associated host galaxy at $z = 0.16$ (Levan 2016). While both have >10 kpc offsets from the center of their host galaxies, these intrinsic offsets are within the offset distribution for SGRBs (see Fong et al. 2015 for a compiled sample) and both putative host galaxies are large (giving reasonable offsets when normalized by the light radius of the host galaxy). From both visual inspection of the lightcurves, runs of the Targeted Search, and time-resolved spectral analysis, neither GRB 080905A nor GRB 160821B have obviously distinct tails. For reasons previously discussed, this is not necessarily surprising. Both SGRBs are about a second long, and the soft tails may cool out of band before the main emission ends. Additionally, because GBM is a background-dominated instrument at low energies, shorter transients are more easily distinguished from background. Therefore, it is more difficult to distinguish comparatively weak soft emission over longer timescales that would be expected for these two bursts if the relative timescales hold. The soft emission may also be undetectable in these bursts given the relative $L_{\text{iso}}^{\text{ST}}$ values

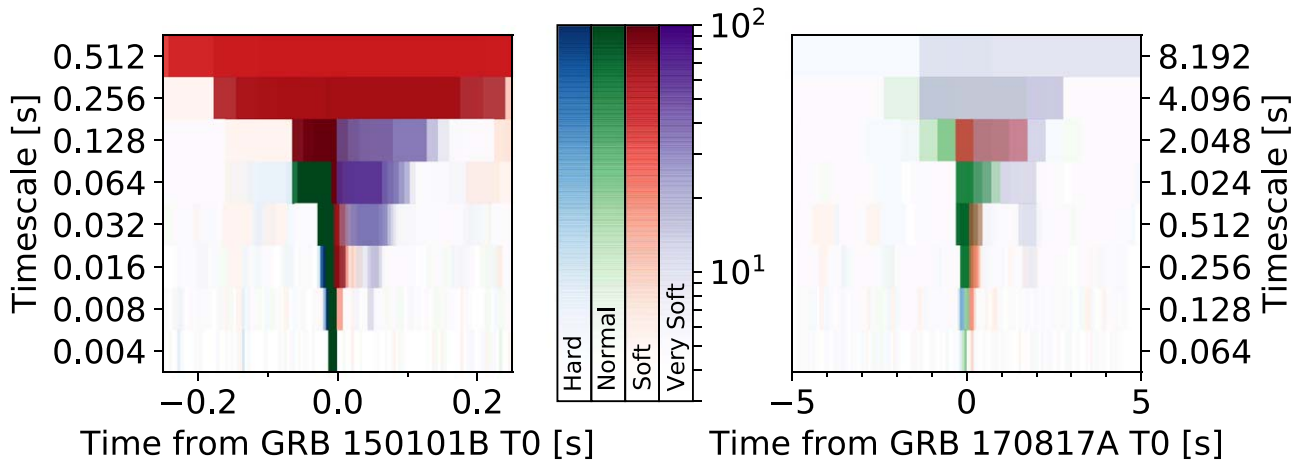


Figure 4. Similarity of GRBs 150101B (left panel) and 170817A (right panel) in a single image: the spectrally separated waterfall plots from the GBM Targeted Search runs. Times are relative to the trigger times of the respective bursts. The four templates used here include three GRB-like spectra (the hard shown in blue, normal in green, and soft in red) and one very soft thermal template (shown in purple; $kT = 10$ keV). The color maps show the log likelihood ratio for that template; all are fixed to the same range. This last template was added in response to the discovery of the soft tail in GRB 170817A. The bursts are phenomenologically similar.

compared to $L_{\text{iso}}^{\text{MP}}$ for GRBs 150101B and 170817A; i.e., they occur at a distance where the main peak is detectable but the soft tail is not recoverable. If the soft component is of cocoon origin, then the luminosity of the soft tail may depend on the uncertain ejecta density or the external density into which the jet and cocoon propagate. These densities may vary considerably between SGRBs, resulting in a wide range of luminosities for the secondary soft tails. It may also be that these bursts just do not have soft tails.

6. Conclusion

GRB 170817A was certainly a unique burst: the second multimessenger astrophysical transient (after SN1987A, see Hirata et al. 1987), long and soft for a SGRB, subluminous, the first with a distance measured by GWs, the closest SGRB with a known distance, and the apparent two-component nature. GRB 150101B is short and hard, has unexceptional properties detected at Earth, is one of the closest SGRBs, and has the same apparent two-component nature of the prompt gamma-rays as GRB 170817A. Troja et al. (2018b) argued that the follow-up observations of GRB 150101B show similarities to GRB 170817A.

Finding an unusual observational signature in one transient is extremely interesting. Finding the same two-component signature in prompt gamma-rays in a second nearby SGRB suggests that it may be a common feature. If the soft tail is an intrinsic property of SGRBs it may have been previously unrecognized due to the lack of detectability (because it is subdominant to the main emission or the distance to the source too great) or may lie hidden in the data owing to insufficiently targeted analysis techniques. It may be more difficult, or even impossible, to detect in instruments that are less sensitive or with a higher low-energy threshold than GBM.

SGRBs with extended emission (see, e.g., Lazzati et al. 2001; Connaughton 2002; Norris & Bonnell 2006) are SGRBs with a usual short hard spike and fainter emission lasting for tens to ~ 100 s, where the extended emission may have a higher fluence than the short spike. It appears unlikely that this emission is similar to the soft thermal-like tails observed in GRBs 150101B and 170817A. Extended emission tends to be softer than the hard spike, but some have peak energies of

several hundred keV (e.g., Kaneko et al. 2015; Svinkin et al. 2016); in some cases the peak energies of the extended emission exceeds that of the main pulse (Svinkin et al. 2016). Some fits of extended emission can constrain spectral curvature and give low-energy power-law indices similar to those observed for GRBs (Kaneko et al. 2015; Svinkin et al. 2016), which is dissimilar to the values expected for comptonized fits of a blackbody spectrum. No previously identified SGRB with extended emission appears similar to GRBs 150101B or 170817A, but these investigations predate GRB 170817A. A careful examination of the *Fermi* GBM SGRB population will provide insight into the commonality and origin of the soft tail. The search of the full GBM SGRB population is the subject of an ongoing study, and will be informed by the results of this work.

While SGRBs have been observed for 50 years, neutron star mergers are now studied in new ways as both GWs and kilonovae. GW observations provide a distance measure free from the ambiguity of associating SGRBs with their host galaxies in the nearby universe (Tunnicliffe et al. 2014), a time and location to seed the GBM Targeted Search (enabling the detection of GRB 170817A-like events to greater distances, see Goldstein et al. 2017), and provide direct observations of the central engine unavailable to electromagnetic observatories. Further, while GRB observations can suggest one of the compact object progenitors is a neutron star, GW or kilonova observations may be able to distinguish between binary neutron star and neutron star–black hole mergers. Cocoon emission may always arise for binary neutron star mergers, but is not expected to occur for neutron star black hole mergers as they likely have lower densities at their polar regions (Metzger 2017), where the jet is believed to originate. Therefore, future multimessenger observations may determine if the soft tail arises from a cocoon.

However, if the soft tail is confirmed with future observations or more careful analysis of existing observations, and is generally subdominant, it will be a key observational signature to identify nearby events from the prompt gamma-ray emission alone, regardless of the physical mechanism. This would enable the prioritization of follow-up GW searches or electromagnetic follow-up observations shortly after the time of the merger, and provide unique insights into the physics of neutron star mergers.

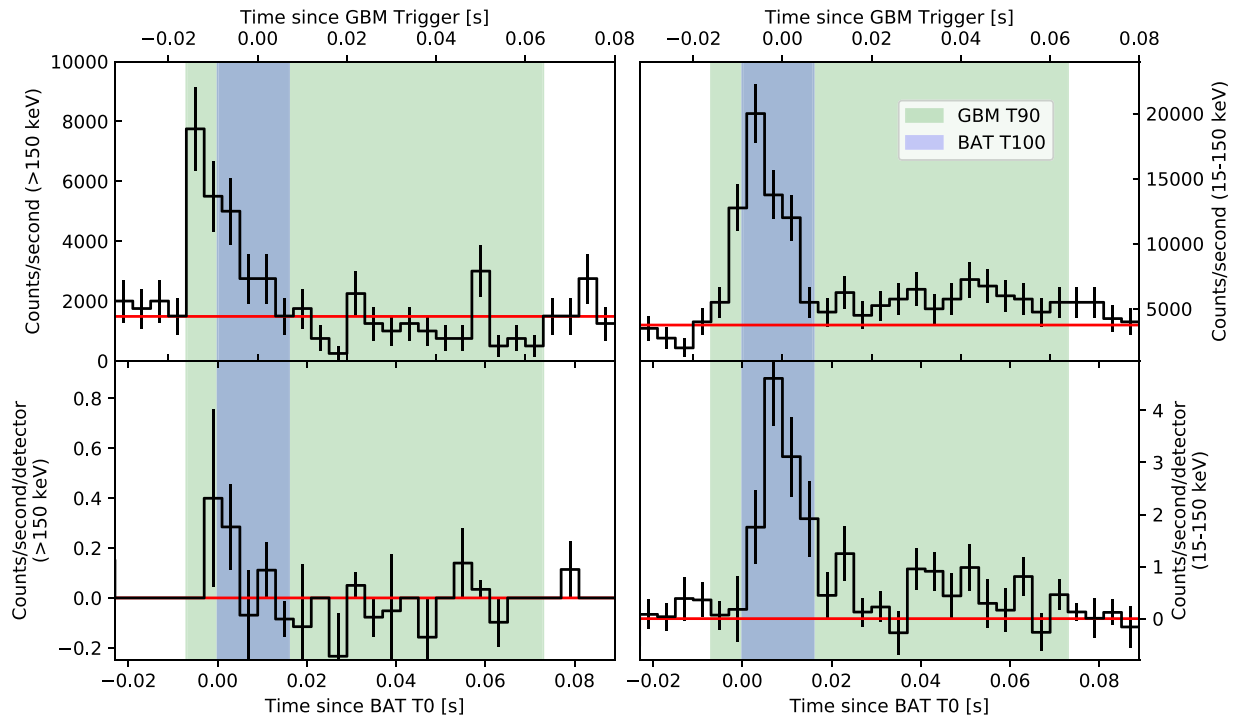


Figure 5. Counts lightcurves for GRB 150101B as observed by *Fermi* GBM (top) and *Swift* BAT (bottom) in the 15–150 keV (right) and >150 keV energy ranges (left). Shown are 4 ms lightcurves in black and a background estimate in red. Time axis values are relative to the T_0 times of each instrument (GBM on top with T_0 defined as the trigger time, and BAT on bottom with T_0 defined as the start of the T100 interval since BAT did not trigger on-board). The lightcurves are aligned by correcting for light travel time between *Fermi* and *Swift* (a difference of 1.35 ms, with the burst arriving at *Swift* first). The standard duration measure of each instrument are shown with the BAT T100 interval in blue and the GBM T_{90} interval in green.

The authors thank the referee for valuable comments and feedback. The authors thank A. Lien for an exhaustive effort to help us understand the differences between the GBM and BAT observations of GRB 150101B. The authors also thank M. Aloy for the combined external shocks and photospheric emission initially presented in Abbott et al. (2017a). The USRA co-authors gratefully acknowledge NASA funding through contract NNM13AA43C. The UAH co-authors gratefully acknowledge NASA funding from co-operative agreement NNM11AA01A. E.B. and T.D.C. are supported by an appointment to the NASA Postdoctoral Program at the Goddard Space Flight Center, administered by Universities Space Research Association under contract with NASA. D.K., C.A.W.H., C.M.H., and T.L. gratefully acknowledge NASA funding through the *Fermi* GBM project. Support for the German contribution to GBM was provided by the Bundesministerium für Bildung und Forschung (BMBF) via the Deutsches Zentrum für Luft und Raumfahrt (DLR) under contract number 50 QV 0301. A.v.K. was supported by the Bundesministeriums für Wirtschaft und Technologie (BMWi) through DLR grant 50 OG 1101. N.C. acknowledges support from NSF under grant PHY-1505373.

Appendix

Other Prompt Gamma-Ray Observations of GRB 150101B

GRB 150101B triggered *Fermi* GBM on-board (Stanbro 2015) and was found in ground searches of the data from the *Swift* Burst Alert Telescope (BAT; Cummings 2015) and two instruments on *INTEGRAL* (Rodi 2018).

Although *Swift* BAT and *Fermi* GBM have comparable sensitivities to SGRBs (Burns et al. 2016), GRB 150101B did not trigger the BAT instrument because the *Swift* spacecraft was slewing at the time it occurred. The initial circular

(Cummings 2015) localized the burst to (R.A., decl.) = (188.044, -10.956) and reported a single peak structure with a T_{90} of ~ 18 ms. Two spectral fits were described: a blackbody with $kT = (10 \pm 2)$ keV and a power law with photon index (3.3 ± 1.5) , exceptionally soft for a SGRB. Additionally, a significant spectral lag was reported, which is rare for SGRBs. With the knowledge of the analysis presented here, this lag may be due to the second component which was not independently identified in the BAT data. At the time of detection the lag contributed to an ambiguous characterization of the event and the initial BAT circular did not conclusively classify it as a GRB. The event does appear in the Third *Swift* BAT GRB Catalog (Lien et al. 2016), which reports a power law fit measured over the burst duration of 16 ms with an index of -1.5 , which is more typical for SGRBs and consistent with the power-law index from the GBM catalog.¹⁴

In Burns et al. (2016), we previously investigated the observational differences of GRB 150101B as seen by BAT and GBM. We present here a fuller understanding, that is aided by Figure 5. The 16 ms interval from the BAT Catalog is not the same as the 16 ms of the main peak as observed by GBM. After accounting for the relative trigger times and the light travel time, the BAT 16 ms interval starts several ms after the GBM interval. There is evidence for both emission episodes in BAT. The BAT energy range is narrower at both the low and high ends compared to *Fermi* GBM (15–150 keV compared to 8 keV–40 MeV). As shown in Figure 3 and Table 1, the start of the main peak has a higher peak energy, higher energy flux, and lower photon flux than the end of the main peak, which may explain the lack of significant signal in BAT at the start of the burst. There is a hint of the hard emission above 150 keV in

¹⁴ <https://heasarc.gsfc.nasa.gov/W3Browse/fermi/fermigbrst.html>.

BAT, during the main peak identified by GBM. This emission is captured by the GBM measure of duration as it is performed in flux space. The BAT calculation of duration is performed in counts space, where the measure is dominated by the more numerous lower-energy counts. This is also a result of GBM having a larger effective area at higher energies than BAT. There is also evidence for the soft emission in BAT: the initial fits reported in Cummings (2015) and the fits reported in Troja et al. (2018b) prefer a blackbody, consistent with the GBM observations of the soft tail. However, the soft tail was not independently identified in *Swift* BAT. The source position was at a good geometry for *Fermi* GBM, with 5 NaI and both BGO detectors having good views. The source position occurred at $\sim 40\%$ partial coding fraction for *Swift* BAT. The soft tail may be less significant in BAT due to the sensitivity of each instrument to the source position at trigger time and the higher low-energy limit of the BAT. The authors of Troja et al. (2018b) reached similar conclusions on the differences between the BAT and GBM observations of GRB 150101B (private communication).

In response to Troja et al. (2018b), observations of GRB 150101B by the *INTEGRAL* spacecraft were recently reported (Rodi 2018). The *INTEGRAL* team report marginal detections in SPI-ACS and IBIS-PICsIT. SPI-ACS data is 50 ms long, which is a factor of a few longer than the 16 ms main peak measured in GBM data. Despite this, a sharp spike is observed. As SPI-ACS has increased sensitivity at higher energies and no sensitivity below 75 keV, this confirms the existence of spectrally hard emission in GRB 150101B.

GRB 150101B has high flux and a high peak energy and was within the field of view of the *Fermi* Large Area Telescope (LAT) at event time, but there is no significant detection in the LAT.

ORCID iDs

P. Veres  <https://orcid.org/0000-0002-2149-9846>
 J. Racusin  <https://orcid.org/0000-0002-4744-9898>
 A. Goldstein  <https://orcid.org/0000-0002-0587-7042>
 E. Bissaldi  <https://orcid.org/0000-0001-9935-8106>
 W. S. Paciesas  <https://orcid.org/0000-0002-2481-5947>
 C. A. Wilson-Hodge  <https://orcid.org/0000-0002-8585-0084>

References

Aasi, J., Abbott, B. P., Abbott, R., et al. 2015, *CQGra*, 32, 074001
 Abbott, B., Abbott, R., Abbott, T., et al. 2017a, *ApJL*, 848, L13
 Abbott, B., Abbott, R., Abbott, T., et al. 2017b, *ApJ*, 841, 89
 Abbott, B., Abbott, R., Abbott, T., et al. 2018a, arXiv:1805.11579
 Abbott, B. P., Abbott, R., Abbott, T., et al. 2018b, *LRR*, 21, 3
 Abbott, B. P., Abbott, R., Abbott, T. D., et al. 2017c, *PhRvL*, 119, 161101
 Acernese, F., Agathos, M., Agatsuma, K., et al. 2015, *CQGra*, 32, 024001
 Ackermann, M., Asano, K., Atwood, W., et al. 2010, *ApJ*, 716, 1178
 Alexander, K., Berger, E., Fong, W., et al. 2017, *ApJL*, 848, L21
 Alexander, K., Margutti, R., Blanchard, P., et al. 2018, arXiv:1805.02870
 Barsotti, L., Fritschel, P., Evans, M., & Gras, S. 2018, LIGO DCC, <https://dcc.ligo.org/LIGO-T1800044/public>
 Bauswein, A., Gorieli, S., & Janka, H.-T. 2013, *ApJ*, 773, 78
 Blackburn, L., Briggs, M. S., Camp, J., et al. 2015, *ApJS*, 217, 8
 Bloom, J. S., Frail, D. A., & Sari, R. 2001, *ApJ*, 121, 2879
 Bromberg, O., Tchekhovskoy, A., Gottlieb, O., Nakar, E., & Piran, T. 2017, *MNRAS*, 475, 2971
 Burns, E. 2017, PhD thesis, Univ. Alabama in Huntsville

Burns, E., Connaughton, V., Zhang, B.-B., et al. 2016, *ApJ*, 818, 110
 Connaughton, V. 2002, *ApJ*, 567, 1028
 Cummings, J. R. 2015, GCN, 17267, 1
 Finn, L. S., & Chernoff, D. F. 1993, *PhRvD*, 47, 2198
 Finstad, D., De, S., Brown, D. A., Berger, E., & Biwer, C. M. 2018, *ApJL*, 860, L2
 Fong, W., Berger, E., Margutti, R., & Zauderer, B. A. 2015, *ApJ*, 815, 102
 Fong, W.-f., Margutti, R., Chornock, R., et al. 2016, *ApJ*, 833, 151
 Goldstein, A., Burns, E., Hamburg, R., et al. 2016, arXiv:1612.02395
 Goldstein, A., Veres, P., Burns, E., et al. 2017, *ApJL*, 848, L14
 Golkhou, V. Z., Butler, N. R., & Littlejohns, O. M. 2015, *ApJ*, 811, 93
 Goodman, J. 1986, *ApJL*, 308, L47
 Gottlieb, O., Nakar, E., Piran, T., & Hotokezaka, K. 2017, *MNRAS*, 479, 588
 Gottlieb, O., Nakar, E., Piran, T., & Hotokezaka, K. 2018, *MNRAS*, 479, 588
 Gruber, D., Goldstein, A., von Ahlefeld, V. W., et al. 2014, *ApJS*, 211, 12
 Guirrec, S., Briggs, M. S., Connaughton, V., et al. 2010, *ApJ*, 725, 225
 Haggard, D., Nynka, M., Ruan, J. J., et al. 2017, *ApJL*, 848, L25
 Hirata, K., Kajita, T., Koshiba, M., et al. 1987, *PhRvL*, 58, 1490
 Jenke, P., Linares, M., Connaughton, V., et al. 2016, *ApJ*, 826, 228
 Kaneko, Y., Bostanci, Z., Göğüş, E., & Lin, L. 2015, *MNRAS*, 452, 824
 Kaneko, Y., Preece, R. D., Briggs, M. S., et al. 2006, *ApJS*, 166, 298
 Kasliwal, M., Nakar, E., Singer, L., et al. 2017, *Sci*, 358, 1559
 Kocevski, D., Burns, E., Goldstein, A., et al. 2018, arXiv:1806.02378
 Lazzati, D., Deich, A., Morsony, B. J., & Workman, J. C. 2017, *MNRAS*, 471, 1652
 Lazzati, D., Perna, R., Morsony, B. J., et al. 2018, *PhRvL*, 120, 241103
 Lazzati, D., Ramirez-Ruiz, E., & Ghisellini, G. 2001, *A&A*, 379, L39
 Levan, A., Hjorth, J., Wiersema, K., & Tanvir, N. R. 2015, GCN, 17281, 1
 Levan, A., Wiersema, K., Tanvir, N. R., et al. 2016, GCN, 19846, 1
 Lien, A., Sakamoto, T., Barthelmy, S. D., et al. 2016, *ApJ*, 829, 7
 Lyman, J., Lamb, G., Levan, A., et al. 2018, arXiv:1801.02669
 Margutti, R., Berger, E., Fong, W., et al. 2017, *ApJL*, 848, L20
 Meegan, C., Lichti, G., Bhat, P., et al. 2009, *ApJ*, 702, 791
 Mészáros, P., & Rees, M. J. 2000, *ApJ*, 530, 292
 Metzger, B. D. 2017, *LRR*, 20, 3
 Mooley, K., Deller, A., Gottlieb, O., et al. 2018a, arXiv:1806.09693
 Mooley, K., Nakar, E., Hotokezaka, K., et al. 2018b, *Natur*, 554, 207
 Nakar, E., & Piran, T. 2018, *MNRAS*, 478, 407
 Nakar, E., & Sari, R. 2012, *ApJ*, 747, 88
 Norris, J. P., & Bonnell, J. T. 2006, *ApJ*, 643, 266
 Nynka, M., Ruan, J. J., & Haggard, D. 2018, arXiv:1805.04093
 Panaitescu, A., & Kumar, P. 2000, *ApJ*, 543, 66
 Pe'er, A., Mészáros, P., & Rees, M. J. 2006, *ApJ*, 652, 482
 Planck Collaboration, Ade, P. A. R., Aghanim, N., et al. 2016, *A&A*, 594, A13
 Preece, R. D., Briggs, M. S., Mallozzi, R. S., et al. 2000, *ApJS*, 126, 19
 Ramirez-Ruiz, E., Celotti, A., & Rees, M. J. 2002, *MNRAS*, 337, 1349
 Rhoads, J. E. 1999, *ApJ*, 525, 737
 Rodi, J., Bazzano, A., Ubertini, P., et al. 2018, GCN, 22889, 1
 Rowlinson, A., Wiersema, K., Levan, A., et al. 2010, *MNRAS*, 408, 383
 Ruan, J. J., Nynka, M., Haggard, D., Kalogera, V., & Evans, P. 2018, *ApJL*, 853, L4
 Ryde, F. 2005, *ApJL*, 625, L95
 Savchenko, V., Ferrigno, C., Kuulkers, E., et al. 2017, *ApJL*, 848, L15
 Scargle, J. D., Norris, J. P., Jackson, B., & Chiang, J. 2013, *ApJ*, 764, 167
 Sonbas, E., MacLachlan, G. A., Dhuga, K. S., et al. 2015, *ApJ*, 805, 86
 Stanbro, M. e. a. 2015, GCN, 17276, 1
 Svinkin, D., Frederiks, D., Aptekar, R., et al. 2016, *ApJS*, 224, 10
 Troja, E., Piro, L., Ryan, G., et al. 2018a, *MNRAS Letters*, 478, L18
 Troja, E., Piro, L., van Eerten, H., et al. 2017, *Natur*, 551, 71
 Troja, E., Ryan, G., Piro, L., et al. 2018b, arXiv:1806.10624v1
 Tunnicliffe, R. L., Levan, A. J., Tanvir, N. R., et al. 2014, *MNRAS*, 437, 1495
 Veres, P., Mészáros, P., Goldstein, A., et al. 2018, arXiv:1802.07328
 von Kienlin, A., Beckmann, V., Rau, A., et al. 2003, *A&A*, 411, L299
 Williamson, A. R., Biwer, C., Fairhurst, S., et al. 2014, *PhRvD*, 90, 122004
 Yu, H.-F., Preece, R. D., Greiner, J., et al. 2016, *A&A*, 588, A135